Local valence and magnetic characteristics of La_2NiMnO_6

Haizhong Guo,[1,*] Arunava Gupta,[2] Maria Varela,[3] Stephen Pennycook,[3] and Jiandi Zhang[1,*,†]
[1]*Department of Physics, Florida International University, Miami, Florida 33199, USA*
[2]*Center for Materials for Information Technology and Department of Chemistry, University of Alabama, Tuscaloosa, Alabama 35487, USA*
[3]*Materials Science and Technology Division, Oak Ridge National Laboratory, Oak Ridge, Tennessee 37831, USA*
(Received 8 February 2009; published 4 May 2009)

Epitaxial thin films of ordered double perovskite La_2NiMnO_6 have been studied by a combination of high-resolution scanning transmission electron microscopy, quantitative electron energy loss spectroscopy, x-ray absorption spectroscopy, and x-ray magnetic circular dichroism (XMCD) spectroscopy. Our results show the nominal oxidation states of Ni and Mn ions to be Ni^{2+} and Mn^{4+} thus the ferromagnetism in ground state is mainly due to Ni^{2+}-O-Mn^{4+} superexchange interactions. In addition, short-range ferromagnetic correlations are observed above the Curie temperature ($T_C \sim 280$ K) from XMCD measurement, which are likely induced by antisite defects against long-range ordering of the Ni/Mn sublattice. The XMCD results also demonstrate that the Ni^{2+} and Mn^{4+} ions are ferromagnetically aligned but exhibit large differences in the spin and orbital contributions to their effective magnetic moments.

DOI: 10.1103/PhysRevB.79.172402 PACS number(s): 75.25.+z, 61.66.−f, 68.37.Ma, 78.70.Dm

Multifunctional double perovskite oxides $La_2BB'O_6$ (B=Ni and Co; B'=Mn) have recently gained much interest both because of their rich physics and prospects for technological applications.[1] Ordering in the double perovskites is generally favored by large differences in ionic radius and formal charge between B and B' and it often leads to functional electrical and magnetic properties due to the B-O-B' interaction.[2] Neutron and x-ray diffraction studies on bulk La_2NiMnO_6 (LNMO) and La_2CoMnO_6 (LCMO) provided evidence for long-range ordering of Ni (Co) and Mn cations, consistent with monoclinic $P2_1/n$ or rhombohedral ($R\bar{3}m$) symmetry.[1,3–5] Large magnetic-field-induced changes in the resistivity and dielectric properties have recently been observed in bulk polycrystalline LNMO at temperatures as high as 280 K—a temperature high enough for realistic device applications such as solid-state thermoelectric (Peltier) coolers.[1]

The magnetic properties of bulk LNMO have been studied over the years in order to gain better understanding of the nature of magnetic exchange interactions in this compound.[1,3–8] It had been suggested that LNMO is a ferromagnetic (FM) semiconductor with ordered Ni and Mn ions and the spin is parallel to the b axis,[1] as compared to the antiferromagnetic and paramagnetic (PM) behaviors of $LaMnO_3$ and $LaNiO_3$, respectively. However, according to the spin states and magnetic interactions, there appear to be several controversies concerning the real nature of magnetic coupling. Goodenough *et al.*[6] initially attributed ferromagnetism in LNMO to Mn^{3+}-O-Ni^{3+} superexchange interactions, where low-spin Ni^{3+} and high-spin Mn^{3+} are both Jahn-Teller ions. On the other hand, Blasse[7] argued that ferromagnetism is entirely due to Mn^{4+}-O-Ni^{2+} superexchange interactions, which is supported by ^{55}Mn NMR (Ref. 8) and neutron diffraction studies.[9] Joly *et al.*[5] more recently showed the existence of two different spin states of Mn and Ni in bulk LNMO samples synthesized at different temperatures, and a charge disproportionation of the type $Mn^{4+}+Ni^{2+} \rightarrow Mn^{3+}+Ni^{3+}$ occurs when the low-temperature synthesized LNMO is annealed at high temperatures. Thus, so far even the basic issues concerning the electronic and magnetic structures have not yet been settled. Since the analysis of neutron data is model dependent, it is valuable to directly obtain the site-specific information on local electronic configuration and magnetic properties. In this Brief Report, we report our studies of the local valence and magnetic structure by using a complementary combination of scanning transmission electron microscopy (STEM), electron energy loss spectroscopy (EELS), x-ray absorption spectroscopy (XAS), and x-ray magnetic circular dichroism (XMCD) spectroscopy.

LNMO films were grown epitaxially on $SrTiO_3$ (STO) (100) and $LaAlO_3$ (LAO) (100) substrates at 750 °C and oxygen partial pressure of 800 mTorr by the pulsed-laser deposition technique. Growth and characterization of highly ordered LNMO thin films have been described in our earlier publications.[10,11] Electron microscopy observations were carried out in an aberration corrected STEM (VG microscopes HB501UX) operated at 100 keV, equipped with a Nion aberration corrector and a Gatan Enfina EELS. Details regarding the oxidation states were obtained from analysis of the EELS data of the O K edge around 530 eV and Mn L edge around 644 eV. XAS and XMCD spectra were performed at the soft x-ray beamlines 4.0.2 and 6.3.1 at the Advanced Light Source, Berkeley, CA. All spectra were recorded in total electron yield mode at 30° grazing incidence in applied field of 0.6 T parallel to the x-ray beam while varying the temperature over a range of 100–300 K. The photon helicity was fixed and the magnetic direction was reversed parallel and antiparallel to it. The spectra were normalized after a constant background subtraction. Magnetization of samples was measured using a superconducting quantum interference device (SQUID) magnetometer [magnetic property measurement system (MPMS), Quantum Design].

Figure 1 shows the temperature (T)-dependence of field-cooling magnetization, showing a FM-to-PM transition with $T_C \sim 280$ K. However, as compared with a simple mean field theory for spontaneous magnetization, the FM-to-PM transition is broad. We have used the expression $M \propto (T_C - T)^{\beta}$ to fit the M(T) curve, shown as green line. The β value calcu-

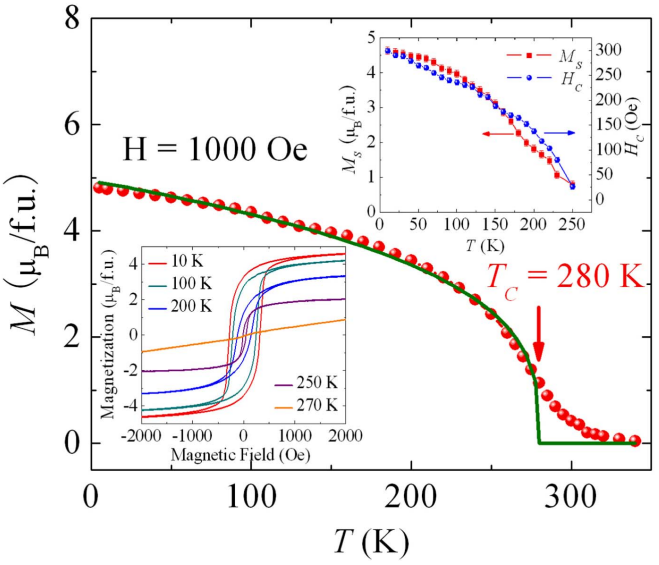

FIG. 1. (Color online) T dependence of the magnetization of LNMO measured in a magnetic field of 1000 Oe. The solid green line is the fitting curve of $M \propto (T_C - T)^{\beta}$ with $\beta \approx 0.31$. The insets present T dependence of $M(H)$ hysteresis loops, the saturation magnetic magnetization, and the coercivity.

lated from the fitting is about 0.31, close to that of the Heisenberg mode,[12] which suggesting that the LNMO belongs to the Heisenberg ferromagnet with short-range couplings. Moreover, an existence of a tail structure on the $M(T)$ curve indicates the possible presence of short-range FM correlations above T_C. The T-dependence of magnetic hysteresis loops, the saturation magnetic magnetization (M_S), and the coercivity (H_C) obtained from the magnetic hysteresis loops are shown in the insets of Fig. 1. Both the saturation magnetization and coercivity decrease with increasing temperature.

The epitaxial nature of film growth and the electronic structure of Mn oxidization state have been characterized with high-resolution STEM and EELS. The results are presented in Fig. 2. The high-resolution Z-contrast images (see the inset of Fig. 2) indicate an excellent unit-cell to unit-cell epitaxial relationship between the film and the substrate.[13] The substrate-film interface is sharp and coherent with no evidence of formation of secondary phases. The only observed imperfection is the existence of antisite defects as described elsewhere in detail.[13] In order to gain insight into the Mn oxidization state of LNMO, we have carried out the EELS measurement of the excitation spectra of Mn $L_{2,3}$ edge of LNMO and the results are shown in Fig. 2. The Mn $L_{2,3}$ edge is attributed to excitations from the spin-orbit split $2p_{3/2}$ and $2p_{1/2}$ core states to higher unoccupied states of Mn $3d$ character. The Mn $L_{2,3}$ edges are expected to shift toward higher energies, increase in intensity, and alter the intensity ratio $I(L_3)/I(L_2)$ of the L_3 by the L_2 peaks with increased Mn valency.[14] The Mn $L_{2,3}$ EELS spectrum measured from LNMO (see Fig. 2) is almost identical to that of $CaMnO_3$ (CMO) but different from that of $LaMnO_3$ (LMO).[15] Our analysis shows that the intensity ratio $I(L_3)/I(L_2)$ of LNMO is $\sim 2.10 \pm 0.15$ which is identical to that of CMO, while the $I(L_3)/I(L_2)$ of LMO is $\sim 2.70 \pm 0.15$.[15] The similarity of Mn $L_{2,3}$ EELS spectra of LNMO and CMO indicates that the oxidation state of Mn in LNMO is Mn^{4+}, suggesting the possible presence of Mn^{4+}-O-Ni^{2+} oxidization structure in the system. Due to the overlaps between the Ni L edge and the La M edge, it is difficult to quantify the Ni oxidization state with EELS.

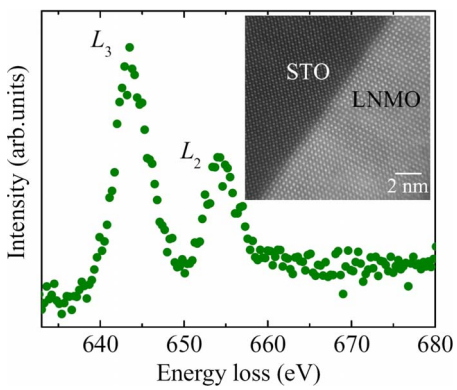

FIG. 2. (Color online) The Mn $L_{2,3}$ EELS spectra of LNMO measured at room temperature. High-resolution STEM image near the interface region is shown in the inset.

Unique to soft x-ray absorption is that the dipole selection rules are very effective in determining which of the $2p^5 3d^{n+1}$ final states are reached and with what intensity, starting from a particular $2p^6 3d^n$ initial state ($n=8$ for Ni^{2+}, $n=7$ for Ni^{3+}, $n=4$ for Mn^{3+}, and $n=3$ for Mn^{4+}). This makes the technique an extremely sensitive local probe, ideal to study the valence[16] and spin[17–19] character in initial states. Figures 3(a) and 3(b) display the photon flux-normalized polarization-dependent Mn $L_{2,3}$ and Ni $L_{2,3}$ XAS spectra I^+ (solid curves) and I^- (dashed curves) for the LNMO thin film taken at 100 (red curves) and 300 K (blue curves). Here, I^+ and I^- refer to the absorption coefficients for the photon helicity parallel and antiparallel to the Mn/Ni $3d$ majority-spin direction, respectively. XMCD spectra ($\Delta I = I^+ - I^-$) are shown in Figs. 3(c) and 3(d). For Mn [see Fig. 3(a)], the spectra correspond to on-site transitions of the form $2p^6 3d^n \rightarrow 2p^5 3d^{n+1}$ and present two groups of multiplets, namely, the L_3 ($\hbar\nu \approx 641-645$ eV) and L_2 ($\hbar\nu \approx 652-656$ eV) white line regions, split by the spin-orbit interaction of the Mn $2p$ core level. The line shape of the spectrum depends strongly on the multiplet structure given by the Mn $3d$-$3d$ and $2p$-$3d$ Coulomb and exchange interactions, as well as the local crystal field effects and the hybridization with the O $2p$ ligands. The Mn $L_{2,3}$ XAS spectra are similar to these measured by Sánchez *et al.*[20] from both $CaMnO_3$ and $LaMn_{0.5}Ni_{0.5}O_3$ but quite different from those observed from $LaMnO_3$. Thus, the Mn $L_{2,3}$ XAS spectra reveal essentially a Mn^{4+} state, consistent with our EELS data. The Ni $L_{2,3}$ edge peaks [Fig. 3(b)] are relatively week and L_3 edge one is overlapped with the very strong La M edge. However, as shown in Fig. 3(e), the line shape of Ni L_2 edge is very similar to that of NiO rather than that of $RNiO_3$ (R=Pr and Nd) (the spectra of NiO, $PrNiO_3$, and $NdNiO_3$ are taken from Ref. 21). The presence of small satellites in Ni L_2 edge is well understood in terms of a covalent ground state of mainly Ni^{2+} ($3d^8$) character plus an anion-dependent fraction of the $3d^9\underline{L}$ and $3d^9\underline{L}^2$ configurations, where $\underline{L}$ stands for an anion (ligand) hole.[21] Therefore, we further confirmed from the Ni $L_{2,3}$ XAS re-

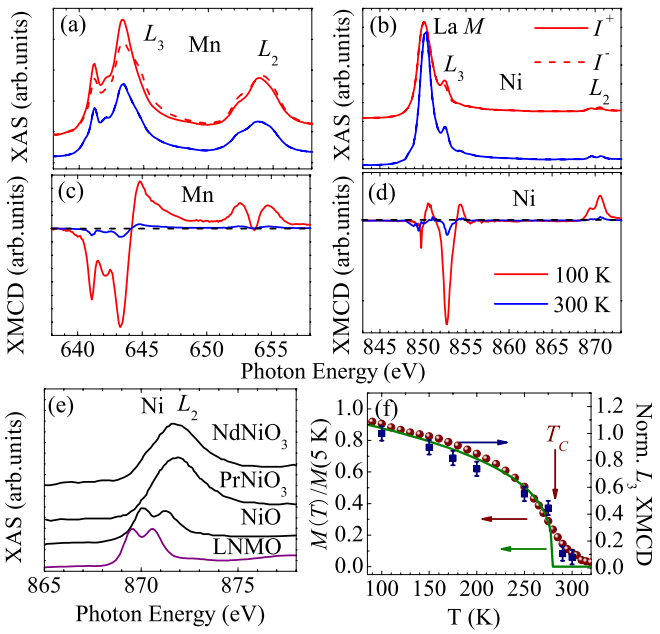

FIG. 3. (Color online) The XAS spectra I^+ (solid) and I^- (dashed) at the edges of (a) Mn $L_{2,3}$ and (b) Ni $L_{2,3}$ and XMCD spectra $\Delta I = I^+ - I^-$ of (c) Mn $L_{2,3}$ and (d) Ni $L_{2,3}$, measured at 100 K (red curves) and room temperature (RT) (blue curves). (e) The enlarged part of the room-temperature Ni L_2 XAS edge of LNMO compared with that of NiO, $PrNiO_3$, and $NdNiO_3$, (which were taken from Ref. 21). (f) T-dependence of the normalized intensity of the Mn L_3 XMCD peak compared with the normalized magnetization $M(T)/M(5\ \mathrm{K})$ and the fitting curve with $M \propto (T_C - T)^{\beta}$ and $\beta \approx 0.31$ [see Fig. 1].

sults that the oxidation states of Ni ions are Ni^{2+}, consistent with the observation of the Mn^{4+} state in the Mn $L_{2,3}$ XAS spectra above, i.e., fulfilling the charge balance requirement. It is important to note that the XMCD is largely negative at both the Ni and the Mn L_3 edges, indicating that the Ni^{2+} and Mn^{4+} ions are aligned ferromagnetically with Mn^{4+}-O-Ni^{2+} superexchange interactions.

The XMCD intensity decreases as the temperature increases without any appreciable change in the spectral line shape, corresponding to the decrease in the magnetization with increasing the temperature [see the T dependence of the normalized intensity of the Mn L_3 XMCD peak compared with the normalized magnetization measured by SQUID in Fig. 3(f)]. It can be seen from Fig. 3 that the normalized $M(T)$ curve exhibits a tail structure and XMCD signals are observed even above T_C, both indicating the presence of short-range FM correlations above T_C. Very recently, the results of electron spin resonance[22] have also revealed the presence of short-range FM correlations above T_C. In addition, an anomalous phonon softening due to spin-phonon coupling in the ferromagnetic state of LNMO was observed extending up to about 400 K, also indirectly suggesting the presence of short-range FM correlations above T_C.[11] First-principles density functional calculations also show the presence of strong coupling between the spins and phonons.[23] The critical behavior of the double perovskite La_2NiMnO_6 has been studied in detail by Lou *et al.*,[12] and they suggested that La_2NiMnO_6 might be a three-dimensional (3D) Heisenberg ferromagnet with short-range interactions.

The orbital magnetic moment μ_{orb} and the spin magnetic moment μ_{spin} of the Mn $3d$ and Ni $3d$ states in the ground state can be estimated by using the XMCD orbital sum rule[24] and spin sum rule,[25]

$$\mu_{\mathrm{orb}} = -\frac{4\left(\int_{L_3}\Delta I(E)dE + \int_{L_2}\Delta I(E)dE\right)}{3\left(\int_{L_3} I(E)dE + \int_{L_2} I(E)dE\right)}(10 - N_{3d}), \quad (1)$$

$$\mu_{\mathrm{spin}} + 7\mu_T = -\frac{2\int_{L_3}\Delta I(E)dE - 4\int_{L_2}\Delta I(E)dE}{\left(\int_{L_3} I(E)dE + \int_{L_2} I(E)dE\right)}(10 - N_{3d}), \quad (2)$$

where N_{3d} is the $3d$ electron occupation number and μ_T is the magnetic-dipole moment which in octahedral symmetry is a small number and negligible compared to μ_{spin}.[26] N_{3d} was deduced from the cluster-model analyses[27] to be 3.8 and 8.2 for Mn^{4+} and Ni^{2+}, respectively. Using these equations, we obtained $\mu_{\mathrm{spin}}^{\mathrm{Mn}} = 2.2165\mu_B/\mathrm{atom}$, $\mu_{\mathrm{orb}}^{\mathrm{Mn}} = 0.0879\mu_B/\mathrm{atom}$, and $\mu_{\mathrm{orb}}^{\mathrm{Mn}}/\mu_{\mathrm{spin}}^{\mathrm{Mn}} = 0.039$ for the Mn $L_{2,3}$ XMCD spectra at 100 K. This means that the orbital moment for the Mn^{4+} ions is nearly quenched. Indeed, for the $3d^3$ configuration in Mn^{4+} compounds, the majority t_{2g} shell is fully occupied without orbital degree of freedom and thus a practically quenched orbital moment is to be expected. The value obtained from the sum rule requires a correction factor due to the large mixing of $j = 3/2$ and $j = 1/2$ levels for the Mn $L_{2,3}$. Edmonds *et al.*[28] used a correction factor of 1.47 then obtained the magnetic moment close to the calculated value for full magnetization. Based on our analysis, the discrepancy should be smaller than 20% in the separation of the integration over each of the spin-orbit split core levels. Therefore a correction factor of 1.2 is more reasonable estimate for our calculation. By using this value of correction factor, we obtain that $\mu_{\mathrm{spin}}^{\mathrm{Mn}} = 2.6598\mu_B/\mathrm{atom}$, $\mu_{\mathrm{orb}}^{\mathrm{Mn}} = 0.1055\mu_B/\mathrm{atom}$, and $\mu_{\mathrm{orb}}^{\mathrm{Mn}}/\mu_{\mathrm{spin}}^{\mathrm{Mn}} = 0.039$. For Ni, we obtained $\mu_{\mathrm{spin}}^{\mathrm{Ni}} = 0.5215\mu_B/\mathrm{atom}$, $\mu_{\mathrm{orb}}^{\mathrm{Ni}} = 0.2188\mu_B/\mathrm{atom}$, and $\mu_{\mathrm{orb}}^{\mathrm{Ni}}/\mu_{\mathrm{spin}}^{\mathrm{Ni}} = 0.246$ at 100 K, which is unexpectedly large for the half-filled $d^8(t_{2g}^6 e_g^2)$ system. It should be noted that the magnetic moments of Ni obtained from the XMCD rules are rather ambiguous as the La M edge has slight XMCD signal. Moreover, the empty La $4f$ states can also be slightly polarized in principle. Figure 4 presents the calculated results based on XMCD data compared with the SQUID-derived M_S. We obtain the total moments $\mu_{\mathrm{tot}} = \mu_{\mathrm{spin}} + \mu_{\mathrm{orb}} \simeq 2.76\mu_B/\mathrm{atom}$ for Mn and $\simeq 0.74\mu_B/\mathrm{atom}$ for Ni. The estimated sum of total magnetic moment $\mu_{\mathrm{TOT}} = \mu_{\mathrm{tot}}^{\mathrm{Mn}} + \mu_{\mathrm{tot}}^{\mathrm{Ni}}$ is $\sim 3.50\mu_B/\mathrm{f.u}$, which is less than the value of M_S ($\sim 4.0\mu_B$) measured at 100 K with SQUID as well as the result ($3.0\mu_B/\mathrm{atom}$ for Mn and $1.43\mu_B/\mathrm{atom}$ for Ni) of the recent spin polarized linear muffin-tin orbital calculations for the system.[23] There are some possible reasons to why the moment in XMCD is

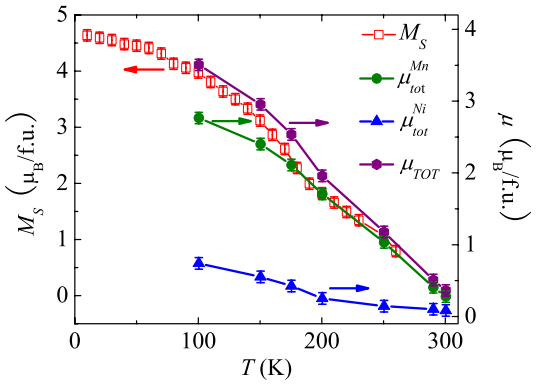

FIG. 4. (Color online) T dependence of the XMCD-derived $\mu_{\mathrm{tot}}^{\mathrm{Mn,Ni}}$ and μ_{TOT} compared with the total moment (M_S) obtained from saturated magnetization measured under 1000 Oe by SQUID.

smaller than that obtained from the SQUID. One reason could be due to a residual moment at O site which is not included in our calculation. Another possible reason could be that the XMCD is very surface sensitive technique for data collection in electron field. Moreover, applying 0.6 T magnetic field along 30° angle with the b axis of the samples could lead to an additional reduction due to the anisotropy. Nevertheless, the T-dependence of XMCD-derived μ_{tot} and μ_{TOT} agrees nicely with that of the SQUID-derived M_S.

To summarize, we have carried out this study of the local valence and magnetic properties of epitaxial thin films of ordered double perovskite La_2NiMnO_6 by using a set of complementary techniques. We have shown that the oxidization state is a Mn^{4+}/Ni^{2+} state in the system so that Ni^{2+}-O-Mn^{4+} superexchange interactions should be responsible for the ferromagnetism in the ground state. In addition, we have revealed the existence of short-range ferromagnetic correlations above $T_C \sim 280$ K, which are likely induced by antisite defects against long-range ordering of the Ni/Mn sublattice. The XMCD results also demonstrate that the Ni^{2+} and Mn^{4+} ions are ferromagnetically aligned in the FM phase but exhibit different spin and orbital contributions to their effective magnetic moments, qualitatively reflecting their different electronic configurations.

This work was supported by NSF under Grant No. DMR-0346826, ONR under Grant No. N000140610226, and NSF NIRT under Grant No. CMS-0609377. The research at ORNL was sponsored by the Office of Basic Energy Sciences, Division of Materials Sciences and Engineering. The authors thank Y. Takamura for helping us in the XAS and XMCD measurements and J. Luck for specimen preparation for STEM.

*Present address: Department of Physics and Astronomy, Louisiana State University, Baton Rouge, Louisiana 70803, USA.
†jiandiz@lsu.edu

[1] N. S. Rogado, J. Li, A. W. Sleight, and M. A. Subramanian, Adv. Mater. (Weinheim, Ger.) **17**, 2225 (2005).
[2] M. Anderson, K. B. Greenwood, G. A. Taylor, and K. R. Poeppelmeier, Prog. Solid State Chem. **22**, 197 (1993).
[3] C. Bull, D. Gleeson, and K. S. Knight, J. Phys.: Condens. Matter **15**, 4927 (2003).
[4] R. I. Dass, J.-Q. Yan, and J. B. Goodenough, Phys. Rev. B **68**, 064415 (2003).
[5] V. L. Joseph Joly, P. A. Joy, S. K. Date, and C. S. Gopinath, Phys. Rev. B **65**, 184416 (2002).
[6] J. B. Goodenough, A. Wold, R. J. Arnott, and N. Menyuk, Phys. Rev. **124**, 373 (1961).
[7] G. Blasse, J. Phys. Chem. Solids **26**, 1969 (1965).
[8] M. Sonobe and K. Asai, J. Phys. Soc. Jpn. **61**, 4193 (1992).
[9] J. Blasco, M. C. Sánchez *et al.*, J. Phys. Chem. Solids **63**, 781 (2002).
[10] H. Guo, J. Burgess, S. Street, A. Gupta, T. G. Calvarese, and M. A. Subramanian, Appl. Phys. Lett. **89**, 022509 (2006).
[11] M. N. Iliev, H. Guo, and A. Gupta, Appl. Phys. Lett. **90**, 151914 (2007).
[12] X. Luo, B. Wang, Y. P. Sun, X. B. Zhu, and W. H. Song, J. Phys.: Condens. Matter **20**, 465211 (2008).
[13] H. Z. Guo, J. Burgess, E. Ada, S. Street, A. Gupta, M. N. Iliev, A. J. Kellock, C. Magen, M. Varela, and S. J. Pennycook, Phys. Rev. B **77**, 174423 (2008).
[14] H. Kurata and C. Colliex, Phys. Rev. B **48**, 2102 (1993).
[15] M. Varela, M. P. Oxley, W. Luo, J. Tao, M. Watanabe, A. R. Lupini, S. T. Pantelides, and S. J. Pennycook, Phys. Rev. B **79**, 085117 (2009).
[16] C. Mitra, Z. Hu, P. Raychaudhuri, S. Wirth, S. I. Csiszar, H. H. Hsieh, H.-J. Lin, C. T. Chen, and L. H. Tjeng, Phys. Rev. B **67**, 092404 (2003).
[17] M. W. Haverkort, Z. Hu, J. C. Cezar, T. Burnus, H. Hartmann, M. Reuther, C. Zobel, T. Lorenz, A. Tanaka, N. B. Brookes, H. H. Hsieh, H. J. Lin, C. T. Chen, and L. H. Tjeng, Phys. Rev. Lett. **97**, 176405 (2006).
[18] S. Ray, A. Kumar, D. D. Sarma, R. Cimino, S. Turchini, S. Zennaro, and N. Zema, Phys. Rev. Lett. **87**, 097204 (2001).
[19] F. Nolting, F. Nolting, A. Scholl, J. Stöhr, J. W. Seo, J. Fompeyrine, H. Siegwart, J.-P. Locquet, S. Anders, J. Lüning, E. E. Fullerton, M. F. Toney, M. R. Scheinfein, and H. A. Padmore, Nature (London) **405**, 767 (2000).
[20] M. C. Sánchez, J. García, J. Blasco, G. Subías, and J. Perez-Cacho, Phys. Rev. B **65**, 144409 (2002).
[21] M. Medarde, A. Fontaine, J. L. Garcia-Munoz, J. Rodriguez-Carvajal, M. De Santis, M. Sacchi, G. Rossi, and P. Lacorre, Phys. Rev. B **46**, 14975 (1992).
[22] S. Zhou, L. Shi, H. Yang, and J. Zhao, Appl. Phys. Lett. **91**, 172505 (2007).
[23] H. Das, U. V. Waghmare, T. Saha-Dasgupta, and D. D. Sarma, Phys. Rev. Lett. **100**, 186402 (2008).
[24] B. T. Thole, P. Carra, F. Sette, and G. van der Laan, Phys. Rev. Lett. **68**, 1943 (1992).
[25] P. Carra, B. T. Thole, M. Altarelli, and X. Wang, Phys. Rev. Lett. **70**, 694 (1993).
[26] Y. Teramura, A. Tanaka, and T. Jo, J. Phys. Soc. Jpn. **65**, 1053 (1996).
[27] T. Saitoh, A. E. Bocquet, T. Mizokawa, and A. Fujimori, Phys. Rev. B **52**, 7934 (1995).
[28] K. W. Edmonds, N. R. S. Farley, T. K. Johal, G. van der Laan, R. P. Campion, B. L. Gallagher, and C. T. Foxon, Phys. Rev. B **71**, 064418 (2005).